

Hybrid linear and non-linear full-waveform inversion of Gulf of Mexico data

Abdullah AlTheyab* and Xin Wang, King Abdullah University of Science and Technology

SUMMARY

Standard Full-waveform inversion (FWI) often suffers from poor sensitivity to deep features of the subsurface model. To alleviate this problem, we propose a hybrid linear and non-linear optimization method to enhance the FWI results. In this method, iterative least-squares reverse-time migration (LSRTM) is used to estimate the model update at each non-linear iteration, and the number of LSRTM iterations is progressively increased after each non-linear iteration. With this method, model updating along deep reflection wavepaths are automatically enhanced, which in turn improves imaging below the reach of diving-waves.

This hybrid linear and non-linear FWI algorithm is implemented in the space-time domain to simultaneously invert the data over a range of frequencies. A multiscale approach is used where higher frequencies are iteratively incorporated into the inversion.

Synthetic data are used to test the effectiveness of reconstructing both the high- and low-wavenumber features in the model without relying on diving waves in the inversion. We apply the method to Gulf of Mexico field data and illustrate the improvements after several iterations. Results show a significantly improved migration image in both the shallow and deep sections.

INTRODUCTION

For deep subsurface imaging, waveform inversion (Tarantola, 1984) should invert deeper reflections and later-arrival refractions rather than first arrivals. Unfortunately, standard FWI has low sensitivity to waveform residuals related to relatively weak deeper reflections compared to the stronger amplitude diving waves. The consequence is slow and often inadequate FWI convergence for reconstructing deep portions of the slowness model. To enhance the sensitivity of FWI to deeper reflections, we use a linear-inversion scheme instead of reverse-time-migration (RTM) (Baysal et al., 1983) for calculating slowness updates. Using this linear inversion, sharp boundaries are incorporated into the slowness model such that they implicitly enhance the model updating along the reflection wavepaths at subsequent iterations. This linear inversion is least-squares reverse-time migration (LSRTM) (Dai et al., 2012).

Using LSRTM, a slowness-perturbation model is computed based on the Born approximation, where the background slowness is fixed during the linear inversion. The slowness model is then updated with the inverted slowness-perturbation model. After that, the linear inversion is repeated with the updated slowness model as a background slowness. Each linear-inversion and updating of the slowness model constitute a non-linear iteration. This combined linear and non-linear inversion procedure is cyclically repeated until acceptable convergence.

This procedure is a variation of Gauss-Newton optimization

for FWI (Akcelik, 2002; Akcelik et al., 2002; Erlangga and Herrmann, 2009; Virieux and Operto, 2009). To avoid high computational and memory costs, the linear inversion is computed by an iterative Conjugate Gradient (CG) solver. The number of CG iterations is increased after each non-linear iteration, and is essential for an accurate model reconstruction. We implemented the algorithm in the time-space domain, and a multiscale approach is used to invert the data for a band of frequencies (Bunks et al., 1995; Boonyasiriwat et al., 2008); starting from a narrow band of low frequencies, and progressively including higher frequencies into the inversion. The term Hybrid FWI encapsulates the concepts of the modified Gauss-Newton optimization with a varying number of CG-iterations, the time-space domain implementation, and the multiscale approach.

In this paper, we review the algorithm for the Hybrid FWI, and illustrate its effectiveness on synthetic data that do not contain diving waves. Then, the Hybrid FWI is also applied to Gulf of Mexico (GOM) data. The resulting tomograms show significant improvements in the deeper section compared to initial solution.

THEORY

Newton's method (Nocedal and Wright, 2006) for minimizing the squared difference $\delta \mathbf{d}$ between the calculated and observed data can be written algebraically as

$$\mathbf{s}_{k+1} = \mathbf{s}_k - \mathbf{H}_f^{-1}(\mathbf{s}_k) \nabla f(\mathbf{s}_k), \quad (1)$$

where \mathbf{s}_k is the slowness model, \mathbf{H}_f is the Hessian matrix and $\nabla f(\mathbf{s}_k)$ is the gradient of the objective function $f(\mathbf{s}_k) = \frac{1}{2} \|\delta \mathbf{d}(\mathbf{s}_k)\|_2^2$ at the k -th iteration. By approximating the Hessian as $\mathbf{H} \approx (\mathbf{J}^T \mathbf{J})$, where \mathbf{J} is the Jacobian matrix, we get the Gauss-Newton optimization formula

$$\mathbf{s}_{k+1} = \mathbf{s}_k - \alpha_k (\mathbf{J}^T \mathbf{J})^{-1} \mathbf{J}^T \delta \mathbf{d}_k. \quad (2)$$

A line search is used to estimate the step length α_k because the approximation of the Hessian might not be an accurate estimate of the curvature for the non-linear misfit function. Instead of inverting the Hessian matrix, we iteratively solve the system of equations

$$(\mathbf{J}^T \mathbf{J}) \mathbf{g} = \mathbf{J}^T \delta \mathbf{d}_k, \quad (3)$$

using the same slowness model to get the search direction \mathbf{g} . In other words, LSRTM is used to compute the search direction \mathbf{g} instead of the RTM. Once the search direction \mathbf{g} and the line-search parameter α are computed, the slowness model is updated using

$$\mathbf{s}_{k+1} = \mathbf{s}_k - \alpha_k \mathbf{g}, \quad (4)$$

and the Jacobian operator and the Hessian matrix are also updated according to the new slowness model. In the following

Hybrid FWI

section, we review the implementation of the Jacobian operator and its adjoint.

Time-domain implementation of the Jacobian and its adjoint

We follow a similar procedure to that of Dai et al. (2012) in deriving a time-domain implementation of applying the Jacobian matrix \mathbf{J} to the slowness perturbation Δs . Each row of the matrix operation $\Delta \mathbf{p} = \mathbf{J} \Delta s$ for calculating wavefield perturbation $\Delta \mathbf{p}$ (indexed by receiver position \mathbf{x}_r and frequency ω) from a slowness perturbation Δs (indexed by spatial position \mathbf{x}) for a given source at position \mathbf{x}_s with a source wavelet $q(\omega)$ is written as

$$\delta p(\mathbf{x}_r, \omega) = 2 \int \omega^2 s_0(\mathbf{x}) \delta s(\mathbf{x}) p_0(\mathbf{x}, \omega) G_0(\mathbf{x}|\mathbf{x}_r, \omega) d\mathbf{x}, \quad (5)$$

where ω is the frequency, s_0 is the background slowness, δs is the slowness perturbation, p_0 is the background incident wavefield from the source, and G_0 is the Green's function. This equation is the solution to the following system of partial differential equations

$$\left(\nabla^2 + \omega^2 s_0^2\right) p_0(\mathbf{x}, \omega) = -\delta(\mathbf{x} - \mathbf{x}_s) q(\omega), \quad (6)$$

$$\left(\nabla^2 + \omega^2 s_0^2\right) \delta p(\mathbf{x}, \omega) = -2\omega^2 s_0 \delta s(\mathbf{x}) p_0(\mathbf{x}, \omega), \quad (7)$$

which indicate that we can evaluate the integral in equation 5 by having two wave-propagation simulations.

Similarly, for the adjoint operation $\Delta s = \mathbf{J}^\dagger \Delta \mathbf{p}$ each row can be written as

$$\delta s(\mathbf{x}) = 2 \iint \omega^2 s_0(\mathbf{x}) p_0(\mathbf{x}, \omega) \times G_0(\mathbf{x}|\mathbf{x}_r, \omega) \delta p^*(\mathbf{x}_r, \omega) d\mathbf{x}_r d\omega. \quad (8)$$

To evaluate this integral, two wavefields are simulated simultaneously by solving the two wave equations:

$$\left(\nabla^2 + \omega^2 s_0(\mathbf{x})^2\right) p_0(\mathbf{x}, \omega) = -\delta(\mathbf{x} - \mathbf{x}_s) q(\omega), \quad (9)$$

$$\left(\nabla^2 + \omega^2 s_0(\mathbf{x})^2\right) R^*(\mathbf{x}, \omega) = -\delta(\mathbf{x} - \mathbf{x}_r) 2\omega^2 \delta p^*(\mathbf{x}_r, \omega). \quad (10)$$

The solution for equation 10 is

$$R^*(\mathbf{x}, \omega) = 2 \int \omega^2 G_0(\mathbf{x}|\mathbf{x}_r, \omega) \delta p^*(\mathbf{x}_r, \omega) d\mathbf{x}_r. \quad (11)$$

By taking the zero-lag correlation and scaling by the background slowness, we get the integral in equation 8, i.e

$$\delta s(\mathbf{x}) = \int s_0(\mathbf{x}) R^*(\mathbf{x}, \omega) p_0(\mathbf{x}, \omega) d\omega = 2 \iint \omega^2 s_0(\mathbf{x}) p_0(\mathbf{x}, \omega) G_0(\mathbf{x}|\mathbf{x}_r, \omega) \delta p^*(\mathbf{x}_r, \omega) d\mathbf{x}_r d\omega. \quad (12)$$

Similar to forward modeling operator, the integral in equation 8 can be evaluated by conducting two wave-propagation

simulations and applying the zero-lag cross-correlation to the two wavefields. The above equations are implemented in the space-time domain for the applications in the following sections.

Physical interpretation of Hybrid FWI

In this section, we develop by example an intuitive reasoning that explains why Hybrid FWI provides more accurate tomograms than standard FWI. Figure 1a shows a block-velocity model which contains one deeper reflector to constrain the shallow velocity anomalies. Because the deep layer has a slower velocity than the shallow layer, it will not generate refractions. Frequencies below 5 Hz are absent from the data as shown in Figure 1b, and the maximum source-receiver offset of 3 km is used for the synthetic data. The initial velocity model is homogeneous with a constant velocity of 2000 m/s. The shallow rectangular anomalies are larger in size than the minimum effective wavelength.

The block model does not generate refractions from the deep interface so that only the reflections from the deeper interface will be employed to reconstruct the square-shaped anomalies. FWI relies on reflections for reconstructing the shallow anomalies, and the velocity updates are attributed to the reflection wavepaths associated with the deep reflector and the boundaries of the anomalies. The construction of reflection wavepaths is dependent on the presence of sharp reflectors in the velocity model. Without the sharp boundaries, standard FWI fails to reconstruct the shallow anomalies as shown in Figure 1c.

LSRTM is known to focus reflections and diffractions into a sharp interfaces in the subsurface model. If such sharp interfaces are incorporated into the velocity model as is the case for Hybrid FWI, these highly resolved reflectors and diffractors generate the wavepaths needed for reconstructing the shallow anomalies. As shown in Figure 1d, the Hybrid FWI make use of reflections, diffractions, multiples and prism waves to construct the anomalies and delineate the boundaries with high resolution. The mispositioning of the deeper reflector due to the shallow velocity error is reduced and the reconstructed reflector is nearly flat. In contrast, the reflectors in the standard FWI tomogram in Figure 1c are more distorted because the deeper reflections are not fully utilized for the same number of iterations. A prohibitively large number of iterations would be needed to accomplish the same results using a non-linear steepest descent optimization method.

APPLICATION TO GOM STREAMER DATASET

We apply the Hybrid FWI to streamer data from the Gulf of Mexico. There are 515 shots with a 37.5 meter shooting interval, and the source-receiver offsets are from 198 meters to 6 kilometers, with a 12.5 meter receiver spacing. The trace length is 10 seconds with a 2 ms sampling interval. Prior to inversion, the data spectra are multiplied by $\sqrt{i/\omega}$ and gained by \sqrt{t} in the time domain to transform 3D to 2D geometric spreading. The source wavelet is estimated by stacking early arrivals from the near-offset traces.

Hybrid FWI

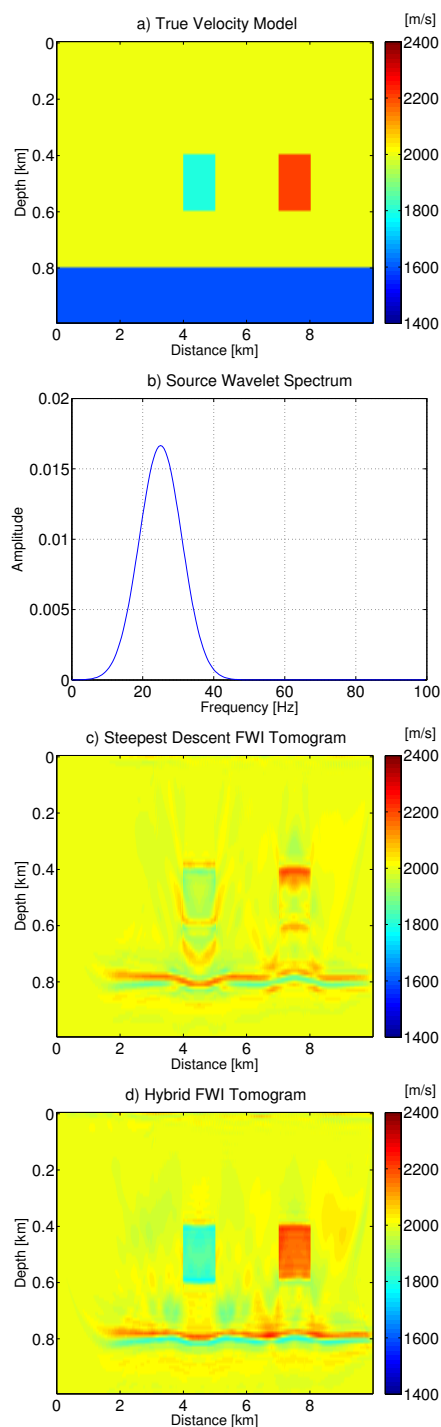


Figure 1: a) Test velocity model, b) the source wavelet spectrum for forward-modeling the synthetic data and inversion, c) steepest descent FWI and d) Hybrid FWI tomograms. The starting velocity model is a constant velocity model with the velocity 2000 m/s, and both of the inversion results have the same computational cost.

We start the inversion with the data bandpassed filtered from 0-4 Hz, because there is reliable signal at 4 Hz. At later iterations, we widened the band of data frequencies to 10 Hz, and Figure 3 shows the initial the final tomograms. The grid size for the tomograms is 301 by 1600 grid points in the vertical and horizontal directions respectively. The grid spacing is 12.5 meters. The inversion is stopped every few non-linear iterations (about 5 iterations) depending on the convergence rate. We stop it if the residual does not decrease by more than 1 percent at every non-linear iteration. We start the inversion again from where we stop with the bandwidth of the observed data widened, and the velocity of the water layer is set to 1500 m/s. Figure 2 shows the convergence curve after the last reset, where the data residual decreases by more than 60 percent.

Figure 4 shows migration images using the initial velocity model and Hybrid-FWI tomogram. The Hybrid-FWI image is more focused. The spliced common-image-gathers (CIG) are flat in the final image, while the CIG's are not flat for the initial image. This highlights the significant improvement to the velocity model. Figure 5 shows two shot gathers from the observed and calculated data and the match is generally good for early arrivals and most of the reflections.

LIMITATIONS AND FUTURE IMPROVEMENTS

A problem with our approach is that the density is assumed to be a constant so that the Hybrid FWI will introduce sharp velocity boundaries with the wrong velocity values. Those boundaries still help in updating the background velocity, which will improve the migration image. Such sharp boundaries can be removed before applying an FWI algorithm which inverts for more subsurface parameters than the acoustic velocity.

We chose to start the inversion with two LSRTM iterations and increase the number of LSRTM iterations by one for every non-linear iteration. Our choice is heuristic based on tests with synthetic data. More work is needed for choosing optimal Hybrid FWI inversion parameters.

CONCLUSION

We implemented and applied the Hybrid linear and non-linear FWI to a GOM dataset. The algorithm uses LSRTM images as slowness updates instead of RTM images. The Hybrid FWI uses the deep reflection data to define sharp boundaries in the velocity model. Those sharp boundaries generate wavepaths that are used by the inversion to build velocity updates for the deeper section. The definition of sharp boundaries and using them in calculating slowness updates are implicit within the algorithm. As a result, the quality of the migration images computed with the Hybrid FWI tomogram appears to be highly resolved at both the shallow and deeper parts.

Hybrid FWI

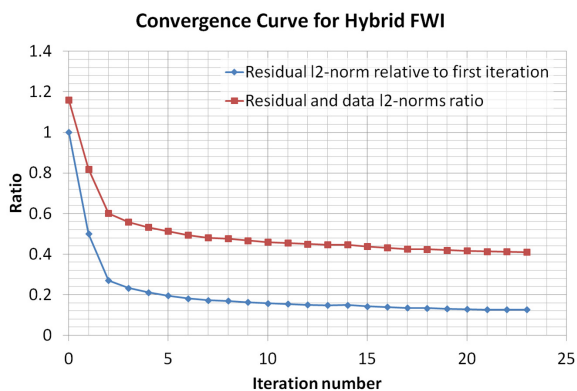


Figure 2: The convergence curves for Hybrid FWI applied to 0-10 Hz GOM data.

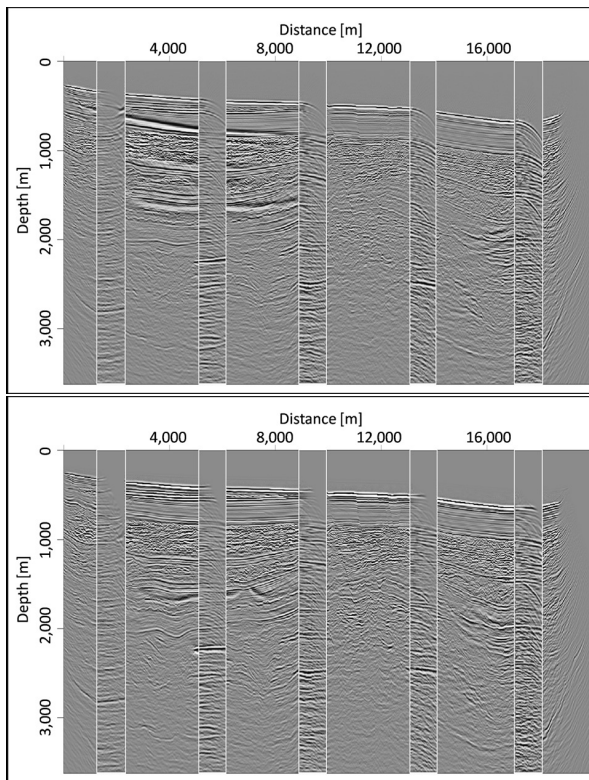


Figure 4: Kirchhoff migration images using the initial velocity model (upper) and the final velocity model (lower). The spliced narrow panels are common image gathers.

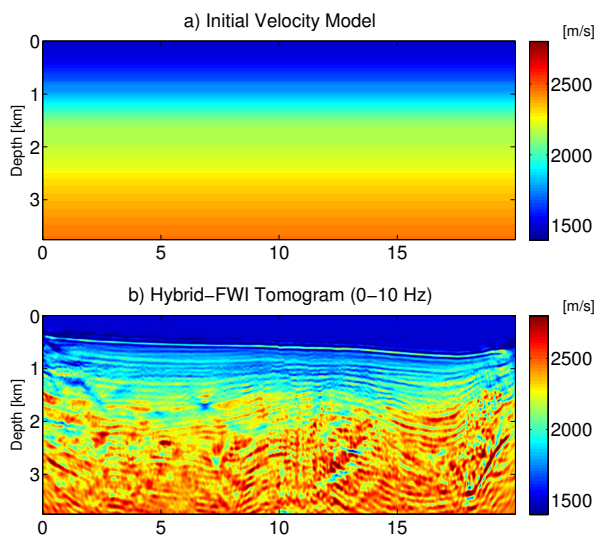


Figure 3: a) the initial velocity model, and b) final Hybrid-FWI tomogram of the band 0-10 Hz.

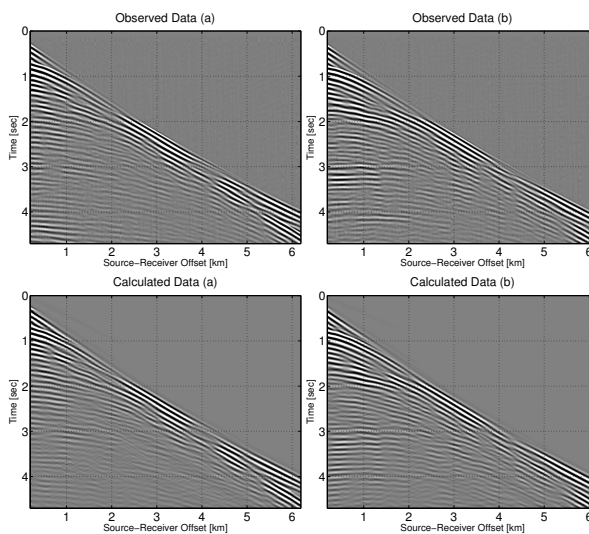


Figure 5: 0-10 Hz shot gathers from different parts of the survey. The observed data are shown in the top panels and the corresponding calculated data at the bottom.

<http://dx.doi.org/10.1190/segam2013-0538.1>

EDITED REFERENCES

Note: This reference list is a copy-edited version of the reference list submitted by the author. Reference lists for the 2013 SEG Technical Program Expanded Abstracts have been copy edited so that references provided with the online metadata for each paper will achieve a high degree of linking to cited sources that appear on the Web.

REFERENCES

- Akcelik, V., 2002, Multiscale Newton-Krylov methods for inverse acoustic wave propagation: Ph.D. thesis, Carnegie Mellon University.
- Akcelik, V., G. Biros, and O. Ghattas, 2002, Parallel multiscale Gauss-Newton-Krylov methods for inverse wave propagation: Supercomputing, ACM/IEEE 2002 Conference, 41.
- Baysal, E., D. D. Kosloff, and J. W. C. Sherwood, 1983, Reverse time migration: *Geophysics*, **48**, 1514–1524, <http://dx.doi.org/10.1190/1.1441434>.
- Boonyasiriwat, C., P. Valasek, P. Routh, B. Macy, W. Cao, and G. T. Schuster, 2008, An application of time-domain multiscale waveform tomography to marine data: 3704–3708.
- Bunks, C., F. Saleck, S. Zaleski, and G. Chavent, 1995, Multiscale seismic waveform inversion: *Geophysics*, **60**, no. 5, 1457–1473, <http://dx.doi.org/10.1190/1.1443880>.
- Dai, W., P. Fowler, and G. T. Schuster, 2012, Multisource least-squares reverse time migration: *Geophysical Prospecting*, **60**, no. 4, 681–695, <http://dx.doi.org/10.1111/j.1365-2478.2012.01092.x>.
- Erlangga, Y. A., and F. J. Herrmann, 2009, Seismic waveform inversion with Gauss-Newton-Krylov method: 79th Annual International Meeting, SEG, Expanded Abstracts, 2357–2361.
- Nocedal, J., and S. J. Wright, 2006, Numerical optimization, 2nd ed.: Springer.
- Tarantola, A., 1984, Inversion of seismic reflection data in the acoustic approximation: *Geophysics*, **49**, 1259–1266, <http://dx.doi.org/10.1190/1.1441754>.
- Virieux, J., and S. Operto, 2009, An overview of full-waveform inversion in exploration geophysics: *Geophysics*, **74**, no. 6, WCC1–WCC26, <http://dx.doi.org/10.1190/1.3238367>.